Optically Pumped GaSb-Based Thin-Disk Laser Design Considerations for CW and Dual-Comb Operation at a Center Wavelength Around 2 μm

Marco Gaulke, Maximilian C. Schuchter, Nicolas Huwyler, Matthias Golling, Benjamin Willenberg, Christopher R. Phillips, and Ursula Keller, *Fellow, IEEE*

***Abstract*—Vertical emitting optically pumped semiconductor laser technology in the GaSb material system, operating in the short-wave infrared (SWIR) regime, has made significant advancements recently. This paper reviews the key achievements leading to the first demonstration of a passively modelocked optically pumped thin-disk semiconductor laser, where both the saturable absorber and the gain quantum wells are integrated into a single semiconductor chip, known as the Modelocked Integrated eXternal-cavity Surface Emitting Laser (MIXSEL). This GaSb-based MIXSEL operates at a center wavelength of 2 μm, supporting both single and dual-comb operations, with an average output power of 30 to 50 mW, pulse repetition rates of approximately 4 GHz, and picosecond pulse durations. It enables initial proof-of-principle dual-comb spectroscopy measurements. For this, we optimized continuous wave (cw) Vertical External Cavity Surface Emitting Laser (VECSEL) operation at 2 μm without an intracavity heatspreader, enhanced group delay dispersion (GDD) compensation, and introduced an additional pump mirror integration. Compared to previous results, we achieved a significant performance increase with pump-DBR 2-μm VECSEL with an average output power of 6 W, an optical pump efficiency of 30% and a reduced thermal resistance of 1.9 K/W. Additionally, the better GDD compensation improved modelocking at 2 μm with a SESAM (Semiconductor Saturable Absorber Mirror), producing near-transform-limited femtosecond pulses with a duration of 331 fs, an average power of 30 mW at a pulse repetition rate of 2.77 GHz. Successful integration of the saturable absorber within the MIXSEL chip required matching of the cavity mode sizes on both the SESAM and the VECSEL chip. This paper details the optimization processes and resulting performance enhancements that mark a significant milestone in the development of GaSb-based thin disk laser technology.**

Received 26 June 2024; revised 14 August 2024; accepted 27 August 2024. Date of publication 4 September 2024; date of current version 7 October 2024. This work was supported by European Research Council (ERC) through European Union's Horizon 2020 Research and Innovation Program under Grant 787097. *(Corresponding author: Marco Gaulke.)*

Marco Gaulke, Nicolas Huwyler, Matthias Golling, Benjamin Willenberg, Christopher R. Phillips, and Ursula Keller are with the Ultrafast Laser Physics Group, Institute for Quantum Electronics, ETH Zürich, 8093 Zürich, Switzerland (e-mail: gaulkem@ethz.ch).

Maximilian C. Schuchter is with the Ultrafast Laser Physics Group, Institute for Quantum Electronics, ETH Zürich, 8093 Zürich, Switzerland, and also with the Optoelectronics Research Centre (ORC), Physics Unit/Photonics, Faculty of Engineering and Natural Sciences, Tampere University, 33720 Tampere, Finland.

Color versions of one or more figures in this article are available at https://doi.org/10.1109/JSTQE.2024.3454521.

Digital Object Identifier 10.1109/JSTQE.2024.3454521

***Index Terms*—Dual-comb generation, GaSb, MIXSEL, modelocking, optically pumped semiconductor laser, SESAM, short-wave-infrared lasers, VECSEL.**

I. Introduction

OPTICALLY pumped continuous wave (cw) semiconductor thin disk lasers, known as Vertical External Cavity Surface Emitting Lasers (VECSELs) [1], support high average power scaling with up to the 100 W in the near infrared [2], [3], [4]. The external cavity design allows for incorporation of additional elements to support intracavity frequency doubling [4], single-frequency operation for quantum applications [5], [6], [7] and passive modelocking with an intracavity SESAM (Semiconductor Saturable Absorber Mirror) [8], [9], [10], [11]. Optical pumping of semiconductor lasers enhances high-beam-quality power scaling by increasing both pump and laser cavity mode sizes on the gain chip.

Since both the SESAM and the VECSEL chip are based on semiconductor epitaxy, the gain and the saturable absorber layers can be integrated into a single chip, forming one end mirror in a straight linear cavity, known as the Modelocked Integrated eXternal-cavity Surface Emitting Laser (MIXSEL) [12], [13]. The pulse repetition rate can be adjusted by the length of the external cavity, ranging from around 1 GHz to 100 GHz [14], [15]. For example, achieving a 3-GHz pulse repetition rate requires a linear cavity length of around 5 cm for fundamental modelocking with only one pulse per cavity roundtrip, which is essential for low-noise operation. Scaling to lower pulse repetition rate becomes more challenging with the onset of multipulse instabilities [16].

A dual-comb MIXSEL has been demonstrated before in the near-infrared [17], and has been utilized for dual-comb spectroscopy in water vapor [18] and acetylene [19] without the need for optical comb stabilization. However, many applications require longer wavelength sources in the short-wave infrared (SWIR) and even mid-infrared range. Relevant trace gases exhibit specific strong absorption features in this range. This enables potential applications such as rapid or high-resolution spectroscopic gas detection for industrial process monitoring and environmental control. Additionally, LiDAR systems operating in the longer wavelength range can be considered eye-safe [20]. Recently, we demonstrated the first dual-comb MIXSEL

© 2024 The Authors. This work is licensed under a Creative Commons Attribution 4.0 License. For more information, see https://creativecommons.org/licenses/by/4.0/

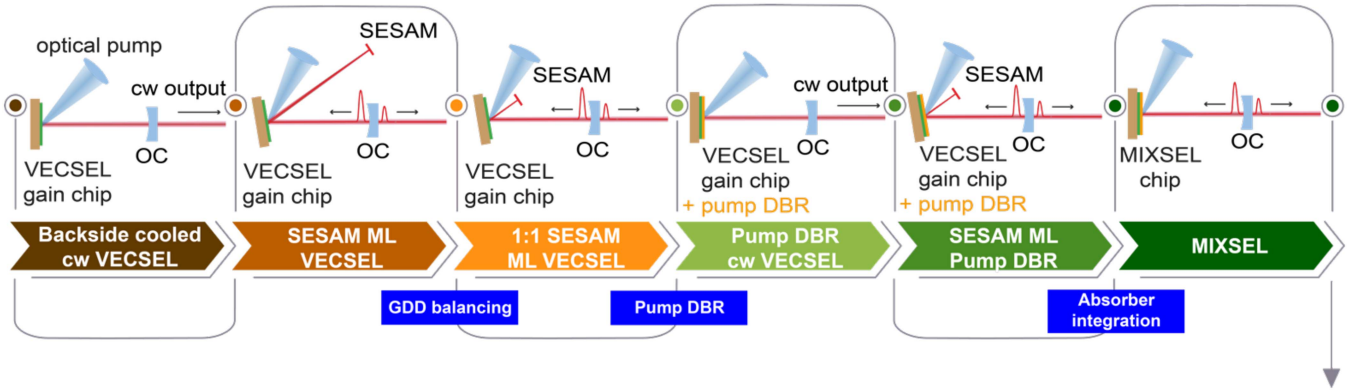

Fig. 1. Milestones in the development of the 2-µm MIXSEL chip. The initial published milestone involves creating a backside cooled cw VECSEL [24] (brown), which subsequently was modelocked (ML) in a SESAM-VECSEL cavity configuration [23]. As a next milestone we had to improve SESAM modelocking with better group delay dispersion (GDD) compensation and balanced cavity mode sizes on both the SESAM and the VECSEL chip, referred to as 1:1 modelocking (orange). The following step involves integrating a pump-DBR into the VECSEL chip and investigating its cw lasing properties (light green). The pump-DBR is crucial for preventing pump light from reaching the saturable absorber layer in the MIXSEL chip. SESAM-modelocking is then demonstrated with the incorporated pump-DBR VECSEL chip. The final step was to integrate the absorber QW into the optimized VECSEL structure, resulting in a MIXSEL that allows for modelocked operation from a straight linear cavity in both single and dual comb operation (dark green) [21].

at a center wavelength of around 2 µm [21] with low-noise performance to support coherent averaging of dual-comb interferograms [22].

In this paper, we review the key technological achievements leading to the successful demonstration of a dual-comb GaSb-based MIXSEL at a center wavelength of around 2 µm. These milestones, which resulted in significant performance increases, include the optimization of backside-cooled cw VECSELs, the integration of a pump mirror, and enhanced dispersion compensation for near-transform-limited pulses from a SESAM-modelocked VECSEL with balanced cavity mode sizes on SESAM and VECSEL chip. Fig. 1 illustrates these key milestones, which will be discussed in detail in this review article and have only been partially published previously [21], [23], [24].

We greatly benefitted from our previous work on GaAs-based VECSELs and MIXSELs operating in the near infrared with respect to our understanding of laser physics [9], [10], [12], [16], [25], [26], [27]. The GaSb material system allows for laser operation to shift from the near-infrared to the SWIR. The primary challenges in this material system include the poor thermal conductivity of the Distributed Bragg Reflectors (DBRs) and Auger recombination [4], which decreases lasing efficiency at longer wavelengths. For example, for an operation wavelength at 1.55 µm, the AlGaAsSb /$AlAs_{0.08}Sb_{0.92}$ DBR exhibits excellent refractive index contrast, whereas the thermal resistance of an 99-% reflector is 627.5 K/W, which is significantly higher than that of the GaAs material system with a thermal resistance of 57.5 K/W [28].

To avoid these thermal challenges, power scaling of GaSb-based VECSELs has mostly been extensively explored, using intracavity heatspreaders for heat removal [29], [30]. In Section II, we will discuss our power scaling efforts of GaSb-based VECSELs without such intracavity heatspreaders. Intracavity heatspreaders act as spectral filters due to their Fabry-Perot etalon effect and thereby tend to negatively affect passive modelocking. Consequently, modelocking results in the GaSb material system are less mature compared to the GaAs system [23], [31].

In Section III we will discuss the key milestone achievements for the GaSb-based MIXSEL demonstration emitting at a center wavelength around 2 µm [21]. With spatial multiplexing [32] using an inverted biprism in transmission, we also obtained low-noise dual-comb operation supporting coherent averaging of interferograms [21]. For this successful demonstration, we used several key milestone results to validate the final MIXSEL chip design as shown in Fig. 1. Fast SESAMs have been optimized with low nonsaturable loss before [33], [34].

In Section IV we discuss an initial proof-of-principle application demonstration using the dual-comb MIXSEL for dual-comb spectroscopy of CO_2 vapor around 2030 nm. The single-cavity approach results in sufficiently low noise to enable coherent averaging without any additional frequency comb stabilization.

II. Power Scaling of GaSb-Based Cw VECSELs

The cw performance of GaSb-based VECSELs operating in the SWIR regime is summarized in Fig. 2. The VECSEL chip for operation around 2 µm typically consists of a highly reflective GaSb/$AlAs_{0.08}Sb_{0.92}$ DBR, which can be grown with high quality and lattice-matched, and strained InGa(As)Sb quantum well (QW) gain layers placed near the antinodes of the standing wave in the linear cavity. Previously, VECSELs with intracavity heatspreaders have demonstrated the best results over a broad wavelength range from 1.8 µm to 2.8 µm [35]. After the first backside cooling approaches in GaSb only showed low-power performance, we have demonstrated the first backside-cooled VECSEL at around 2 µm with more than 500 mW output power [24] using 15 $In_{0.27}Ga_{0.73}Sb$ gain QWs pumped at 1470 nm and a highly reflective DBR using 19 pairs of GaSb/$AlAs_{0.08}Sb_{0.92}$.

Fig. 2 compares the cw performance of various GaSb-based optically pumped VECSELs found in the literature [4], [24], [30], [36], [37], [38], [39], [40], [41], [42], [43], [44], [45], [46], [47], [48], [49], [50], [51], [52]. The backside-cooled VECSEL chip with an integrated pump-DBR in front of the high-reflecting laser DBR is marked with a star and will be discussed in detail

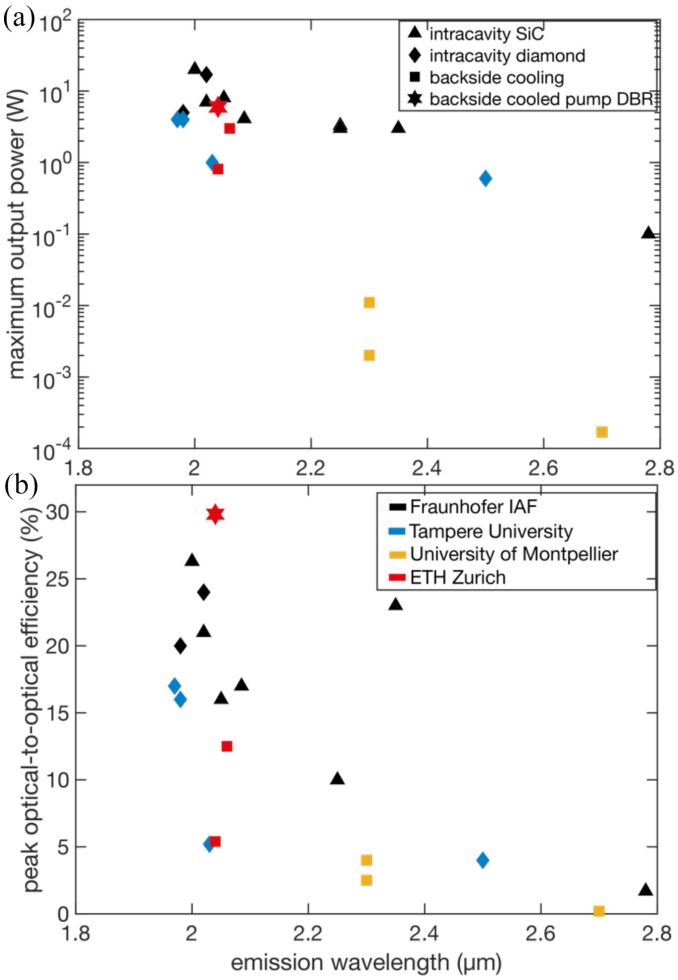

Fig. 2. Average output power (a) and optical-to-optical efficiency (b) of GaSb-based optically pumped VECSELs using various heat removal techniques, including intracavity heatspreaders and backside cooling (squares) with either SiC (triangles) or diamond materials (diamonds). Note that intracavity cooling requires low-loss, high optical-quality heatspreaders. The optical-to-optical efficiencies are shown at the highest output powers. The backside-cooled VECSEL chip with an integrated pump-DBR, discussed in detail in this paper, is marked with a star. The colors denote the research institutes where the results were obtained. This overview considers heatsink temperatures between −15 °C and 20 °C. Typical output coupling rates range from 0.2% to 6%, with higher rates used in multi-gain cavity arrangements. The pump wavelengths range from 0.79 μm to 1.96 μm, with 0.98 μm being the most common.

in this paper. For this result, we also began using quaternary materials to achieve better GDD performance, which is required for modelocking.

Performance depends on the chip temperature and pump wavelength. The chip's temperature directly influences the quantum efficiency of the lasing process, while a longer pump wavelength reduces heating by decreasing the quantum defect. Fig. 2 summarizes the results for various temperatures and pump wavelengths, providing an overview of the general wavelength-dependent trends and characteristics.

The emission wavelength in Fig. 2 ranges from 1.97 μm to 2.78 μm, where the GaSb-material system performs well. For shorter wavelengths, close to the fundamental bandgap of GaSb at 1.7 μm or even lower using aluminum-incorporating alloys, no major issues are expected. However, the InP material system typically performs better at these shorter wavelengths [4]. Extending the wavelength range to longer wavelengths presents significant challenges. As the wavelength increases, Auger recombination considerably reduces lasing efficiency [53], [54]. To extend the wavelength range into the mid-infrared above 3 μm, alternative material systems such as PbSe or PbTe [4], or different QW configurations such as type-II configurations, could be considered [55]. Type-II QWs are standard in electrically pumped interband cascade lasers [56] and have been applied to optically pumped lasers in the GaAs material system [57], [58]. For the current discussion we will only use type-I QWs.

Power and efficiency in Fig. 2 decrease at longer wavelengths, with power dropping from a maximum of approximately 20 W to 0.1 W at 2.78 μm. This decline is due to Auger recombination, reduced hole confinement in the QWs, and the complexities of balancing strain and wavelength in quaternary InGaAsSb QWs. Efficiency similarly decreases, from 30% to nearly 1.7%.

An intracavity heatspreader is a high-quality optical device with stringent requirements regarding loss, surface properties, birefringence, and thermal conductivity. It is typically bonded directly or via capillary techniques very close to the active region, effectively cooling the semiconductor chip. When comparing different intracavity heatspreaders, diamond and silicon carbide (SiC) show similar results. However, diamond is preferred for more output power due to its thermal conductivity being five times higher [30]. However, SiC is commercially available at better surface quality and lower cost, owing to its widespread use in modern power electronics [29].

Overall, intracavity heatspreaders are powerful tools, particularly in material systems with lower thermal conduction. However, they are expensive and can introduce a Fabry-Perot etalon, as observed in many lasing spectra in the literature [30], [43], [45], [46], [47], [49], [52], or cause intracavity losses when they are wedged. Power scaling and efficient cooling are critical topics discussed in these publications. Various aspects are explored, including different heat-spreader materials, pump spot sizes [30], dual-gain and triple-gain cavities [29], [41], [42], [48] and quantum defects at different pump wavelengths [29]. Beam divergence is measured in only a few of these studies. However, the reported values are reasonable, with an M^2 of 1.1-1.6, which tends to increase with higher power [36], [43], [47], [59].

Most of the results focus on adjustable wavelength operation using birefringent filters [36], [42], [43], [45], [46], [47]. These investigations provide estimates of the gain bandwidth under real lasing conditions, achieving tuning ranges of up to 156 nm. We have focused our work on directly measuring the spectral small signal gain and the gain saturation parameters because they are relevant for modelocking [24].

For many applications, single-frequency operation is required, which needs a discussion of possible configurations, their stability, and noise sources [36], [42], [47], [60], [61]. One important application is the development of tunable, low-linewidth lasers for quantum optics experiments [5], [6], [7]. Single-frequency lasers are also interesting for spectroscopy [62], metrology, and communication systems due to their narrow linewidth and stable operation.

Additionally, these optically pumped lasers can serve as single-mode, high-power pumps for holmium, thulium-based, or Cr:ZnSe laser systems [63], [64], [65], [66]. They can also be used to pump nonlinear materials such as periodically poled GaAs or zinc germanium phosphide to create coherent sources at even longer wavelengths [67]. The high output power of up to 20 W enables applications in material processing and medical surgery. Overall, the versatility and high performance of these lasers open up a wide range of potential applications across multiple fields [61].

For wavelengths above 2.3 µm, as shown in Fig. 2, backside cooling techniques cannot compete with intracavity heatspreaders in terms of power and efficiency, which are significantly lower. Here and in the following discussion efficiency refers to optical-to-optical efficiency at the point of highest power and the lowest temperature if different temperatures were measured. However, in recent years, our group has managed to improve the performance of backside-cooled chips, particularly at 2 µm, as indicated by the increased output power and efficiency. The initial enhancement is attributed to improved wafer removal process quality, resulting in up to 800 mW output power [24]. This improvement was targeted at achieving modelocking.

Recently, combining these improved processing techniques with intracavity heatspreaders has led to the development of the first DBR-free membrane external cavity surface emitting laser (MECSEL) in the GaSb material system [59]. This separation of active region and mirror allows for the independent optimization of each component in future projects.

At wavelengths significantly beyond 2 µm, power scaling for backside-cooled devices will likely require replacing the thick lasing DBR with a thinner, highly reflective hybrid metal-semiconductor mirror. We have successfully demonstrated this approach for an operation wavelength at 2 µm, reducing the overall structure thickness by 37%, decreasing thermal resistance from 2.8 to 2.1 K/W, and achieving a maximum cw output power of up to 3 W [37].

Furthermore, incorporating an additional DBR structure into the chip to reflect the pump light has further improved 2-µm VECSELs. The specifics of this chip will be discussed in detail in Section III-B. The maximum output power has reached up to 6 W, with a record-high efficiency of 30%. This efficiency is slightly better than that of a power-optimized device with two heatspreaders [28]. Although the primary goal of incorporating the pump-DBR was not to improve cw operation efficiency, it was to block pump light from penetrating into the rest of the structure, a crucial milestone for developing a MIXSEL where gain QWs and absorbers are integrated into a single structure.

The new milestone results, as shown in Fig. 1, mark significant progress toward a successful implementation of a 2-µm MIXSEL in the GaSb material system. These results are discussed in the following section.

III. Milestones Towards a MIXSEL

Fig. 1 provides an overview of the key milestone achievements for developing a 2-µm MIXSEL chip. We successfully demonstrated the first high-power, backside-cooled GaSb-based VECSEL [24], with subsequent improvements made using a hybrid mirror approach [37]. The GaSb SESAM has been previously optimized for a fast recovery time and low non-saturable loss based on InGaSb QWs embedded in GaSb barriers [33], [34] which was used for our first SESAM-modelocked VECSEL result [23].

The first backside-cooled VECSEL chip [24] did not have any optimization for broadband low GDD. The shortest pulse operation was only achieved by using an additional top-coating on the SESAM structure. This coating compensated for the non-ideal VECSEL GDD, resulting in a flat round-trip GDD in the cavity over a small wavelength region. The thickness variation of the top coating on the SESAM allowed for fine-tuning, ultimately supporting the short 324-fs result [23]. However, the pulses were not transform-limited. Furthermore, we had to focus the laser cavity mode more strongly on the SESAM chip to start to saturate the absorber earlier than the gain accommodating for dynamic gain saturation with an open net gain window. The fluence ratio from VECSEL to SESAM was 1:19.

Within the MIXSEL structure the mode sizes in the saturable absorber and gain cannot be adjusted independently. In addition, we have shown in the GaAs-based system a resonant MIXSEL design with a stronger field enhancement in the absorber versus the gain section is problematic for multiple reasons [68], [69], [70]. Therefore, it is a key milestone result to first achieve a SESAM-modelocked VECSEL with close to equal mode sizes on the SESAM and the VECSEL chip, which we refer to as 1:1 modelocking (i.e., ML stands for modelocking) in Fig. 1. Section III-A explains the GDD and 1:1 modelocking optimization.

The next key achievement is the integration of a pump-DBR which reflects the pump light. Introducing this pump-DBR after the gain structure makes sure that the pump light, does not reach the saturable absorber layer and the highly reflective laser DBR, which contains GaSb layers and therefore also absorbs the residual pump light. Before the full MIXSEL integration, we therefore wanted to first demonstrate pump-DBR integration into the GDD-optimized VECSEL with both cw and modelocking results as described in Section III-B. We achieved significantly improved results compared to earlier publications with this pump-DBR integration for both the cw and SESAM-modelocked VECSEL.

A. Optimized Group Delay Dispersion and 1:1 Modelocking

Fig. 3(a) shows the design of a VECSEL chip engineered to maintain flat and near-zero GDD around its operating wavelength. Both the previous [23] and new designs feature a backside-cooled VECSEL with an antiresonant structure, where the electric field intensity of the lasing wavelength (in red) has a node at the semiconductor-dielectric interface and there is a significantly lower field-intensity enhancement in the gain in comparison to the incoming intensity in air. For the new design (Fig. 3) we did not change the highly reflective laser DBR and the number and spacing of the gain QWs. Specifically, a 19-pair GaSb/$AlAs_{0.08}Sb_{0.92}$ DBR optimized for the laser wavelength is used. The gain region consists of 5x3 $In_{0.27}Ga_{0.73}Sb$ QWs with a thickness of 8 nm embedded into GaSb barrier layers with a thickness of 10 nm. Each of the three QWs are placed around the antinodes of the standing wave.

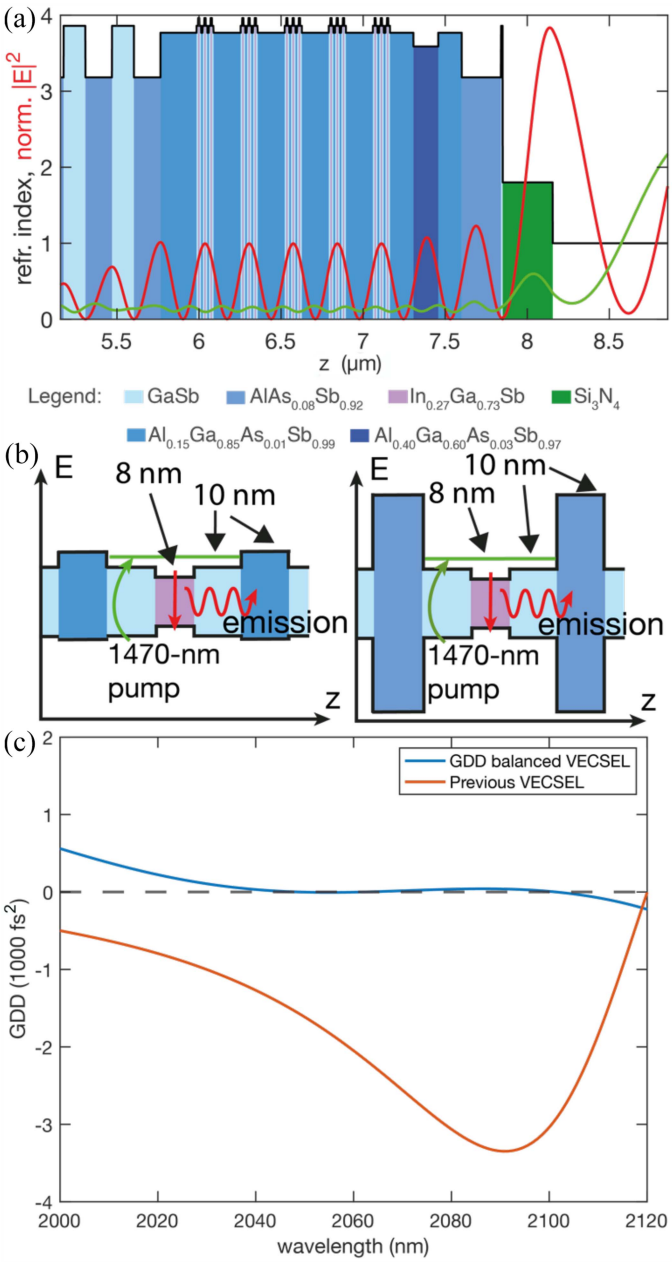

Fig. 3. Properties of a GDD-balanced chip. (a) Design of the active region, showing the refractive index of the materials at the lasing wavelength. The laser DBR is partially depicted. The materials are color-coded with a legend provided at the bottom. The normalized field intensity enhancement is shown for the lasing wavelength (red) and the pump wavelength (green) at their respective angles of incidence. (b) shows the band edges zoomed in on one QW for the new structure on the left and the old structure on the right. The pump is indicated with a green line and the respective thicknesses are indicated. (c) Resulting GDD calculated from the refractive index data using a transfer matrix simulation tool. The GDD of the new chip is shown in blue, while the GDD of the previously used chip for modelocking is shown in red.

To achieve better GDD values, we introduced quaternary materials. The spacer layers between the QW/barrier layers are now grown with $Al_{0.15}Ga_{0.85}AsSb$ instead of $AlAs_{0.08}Sb_{0.92}$ to minimize the refractive index difference and thereby reduce internal reflections from these interfaces. While this adjustment worsens the carrier confinement (Fig. 3(b)) and two-photon absorption properties, it is necessary to balance the GDD. The aluminum content of the $Al_{0.15}Ga_{0.85}AsSb$ spacer layer is selected to minimize the refractive index contrast with the pump absorbing GaSb barrier layer while avoiding absorption of the 1470-nm pump light. Above the active region, a more complex top section with various ternary and quaternary materials is employed to numerically optimize the GDD by fine-tuning their thicknesses. The field intensity enhancement of the pump (in green) is not pronounced because no microcavity resonance is formed and the residual pump light is absorbed in the highly reflective laser DBR, degrading the thermal resistance of this VECSEL chip.

Fig. 3(c) shows the simulated GDD of the optimized VECSEL chip compared to the first design [24]. To perform the simulations, the refractive index dispersion and the bandgap of the quaternary materials were determined via interpolation of the binary and ternary materials. The fine-tuning process involved using a Monte Carlo optimizer combined with a gradient method, allowing the layer thicknesses to vary within specific boundaries. The Monte Carlo optimizer selects random starting parameters within the allowed bounds and minimizes the GDD from each starting point using the gradient method. This search strategy is crucial as it avoids getting stuck in local minima while performing efficiently enough to allow for numerous iterations.

Based on all these design changes, the new VECSEL chip (Fig. 3) exhibits a much flatter and closer-to-zero GDD in the wavelength region of interest, with only slight oscillations around the zero line. In contrast, the first chip [23] had a non-flat GDD with a maximum value exceeding -3000 fs^2, making additional dispersion compensation very challenging. At that time, we used a 1.8-μm thick coating on the SESAM to counteract the non-flat VECSEL GDD and employed a highly dispersive silicon Brewster window to add additional positive GDD to the round-trip GDD.

With the new VECSEL-chip design, the GDD is balanced (Fig. 3(c)), allowing us to use a SESAM with a standard λ/4 Si_3N_4 coating. This slightly increases the field-intensity enhancement in the structure, reducing the saturation fluence and increasing the modulation depth. Now, instead of one component compensating the GDD of another, each component of the cavity has a flat and close-to-zero GDD on its own. This provides more flexibility when changing individual components and investigating modelocking.

This new design also allows for the use of much less dispersive, higher-quality Brewster windows made of YAG or Infrasil to stabilize the polarization in the cavity. For example, a 1-mm YAG window adds only around -147 fs^2 of round-trip GDD compared to $+1560$ fs^2 for a 1-mm silicon window.

The new design also uses quaternary materials, which required substantial additional molecular beam epitaxy (MBE) growth development. Lattice matching of different materials required careful adjustment of the arsenic valve for each material. We had to conduct test runs and perform subsequent characterization using X-ray diffraction measurements. Additionally, different aluminum cell temperatures had to be used within a single run to adjust the aluminum fluxes for the individual materials — $AlAs_{0.08}Sb_{0.92}$, $Al_{0.40}Ga_{0.60}AsSb$, and $Al_{0.15}Ga_{0.85}AsSb$ — present within the same structure. The growth rates also needed to be precisely calibrated prior to each run, as the GDD is highly sensitive to growth rate errors. Even a 1% error in the growth rate of individual materials can accumulate, causing a significant mismatch between the actual and designed GDD, rendering the

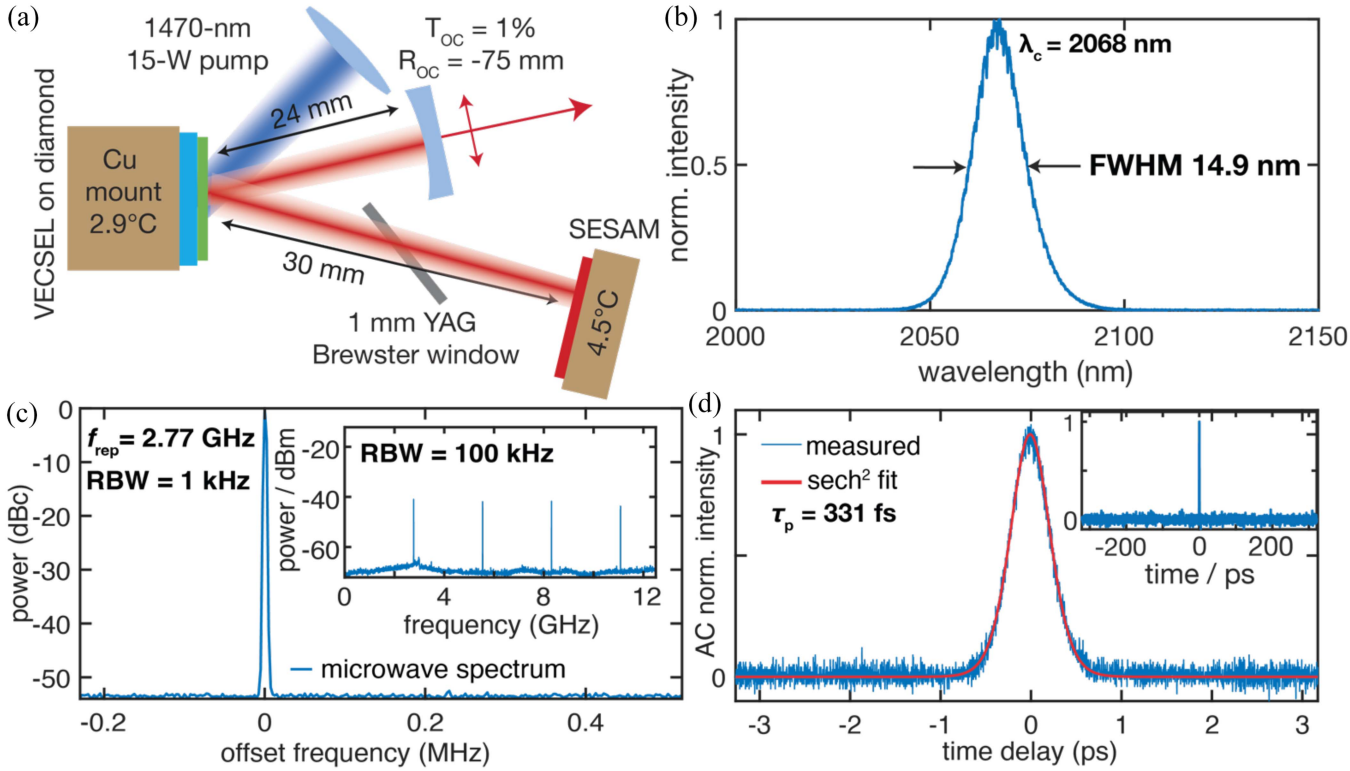

Fig. 4. Modelocking characteristics of the GDD-balanced chip. (a) Modelocking configuration of the V-cavity, including properties of the output coupler (OC), chip temperatures, and pump characteristics. A 1-mm YAG Brewster window is used to stabilize polarization and fine tune the GDD. (b) Optical spectrum centered around 2068 nm with a full-width half-maximum of 14.9 nm. (c) Microwave spectrum recorded using a 10-GHz photodiode at a resolution bandwidth of 1 kHz, zoomed in on the first harmonic, showing a repetition rate of 2.77 GHz. The inset displays the full span of the microwave spectrum, highlighting the higher harmonics. (d) Autocorrelation trace revealing a pulse length of 331 fs, along with a fitted sech^2 function. A wide-scanning autocorrelation is recorded to confirm the absence of any side pulses.

chip unusable for its intended purpose. The margins for errors in modelocked chips are typically much smaller than for cw operation. In cw operation, the QW lasing and the location of the DBR need to match, which is less stringent, allowing for a few percent growth rate errors before the VECSEL stops working.

Fig. 4(a) shows the cavity configuration under which the GDD-balanced VECSEL chip is modelocked with an intracavity SESAM. The chip is flip-chip processed on a diamond heatsink, which is subsequently cooled with a copper mount to 2.9 °C. The pump source is a 1470-nm, 15-W multimode pump diode bar from Lumics with an M^2 of 47. The pump beam is elliptically shaped, resulting in a round spot size of 360 µm in diameter on the chip at a 45° angle of incidence.

The cavity is configured as a V-cavity with a curved 75-mm, 1%-transmission output coupler. Both the SESAM and VECSEL chip are flat mirrors, and the folding angle is approximately 8°. The SESAM is maintained at 4.5 °C, and a 1-mm YAG Brewster window is placed between VECSEL chip and SESAM. The mode size diameters on the SESAM and VECSEL chip are calculated to be 364 µm and 298 µm, respectively. The modelocking ratio is then calculated as the ratio of the two areas, which are proportional to the squares of the diameters and the field intensity enhancements in the structure:

$$1:\mathrm{ML} \;=\; 1:\frac{A_{\mathrm{VECSEL}}\;|E(z)|^2_{\mathrm{VECSEL}}}{A_{\mathrm{SESAM}}\;|E(z)|^2_{\mathrm{SESAM}}}$$

where A_{VECSEL} and A_{SESAM} are the areas of the VECSEL and SESAM, respectively, and $|E(z)|^2$ represents the field intensity enhancement. The field intensity enhancements are calculated at the positions of the QWs and averaged. For the VECSEL chip, this results in a field intensity enhancement of 0.85, and for the SESAM, it is 0.98. Consequently, the modelocking ratio is now 1:1.3, which is significantly closer to 1:1 compared to the previous ratio of 1:19.

The SESAM used is a standard two-quantum-well design with a λ/4 Si_3N_4 anti-reflective coating. It has a saturation fluence of 0.63 µJ/cm^2, a modulation depth of 2.2%, and nonsaturable losses of 0.7%, with a rollover fluence of 2.95 mJ/cm^2 when measured with 120-fs pulses.

Fig. 4(b) shows the optical spectrum of the modelocked, GDD-balanced VECSEL. The optical spectrum is centered around 2068 nm with a full width at half maximum (FWHM) of 14.9 nm. It is only slightly asymmetric and appears clean, indicating stable modelocking. Fig. 4(c) displays the microwave spectrum, zoomed in on the first harmonic at 2.77 GHz. Also, the microwave spectrum is clean, with no side peaks present. The inset reveals the wide scanning microwave spectrum, showing higher harmonics with equal power, except for the fourth harmonic, which decreases due to the 10-GHz cutoff of the 2-µm InGaAs PIN Detector ET-5000F from EOT. Fig. 4(d) presents the autocorrelation measurement, indicating a pulse length of 331 fs, with the inset showing a wide autocorrelation delay scan with no side pulses within the 500-ps scan window.

TABLE I
MODELOCKING RESULTS OF THE GDD-OPTIMIZED VECSEL COMPARED TO PREVIOUS RESULTS OBTAINED WITH A 1:19 MODELOCKING CONFIGURATION

	Previous result	GDD optimized VECSEL
τ_{pulse}	324 fs	**331 fs**
f_{rep}	3 GHz	**2.77 GHz**
λ	2061 nm	**2068 nm**
output power	38 mW	**30 mW**
chirp	0.45 (1.41 x sech^2)	**0.34 (1.08 x sech^2)**

These diagnostics collectively indicate clean modelocking at an output power of 30 mW with a pump power of 4.9 W. The characteristics are summarized in Table I. The mode-locking performance is comparable to previous results [23] with similar pulse length, repetition rate, center wavelength, and output power. However, the chirp is now significantly reduced, resulting in nearly transform-limited pulses with only an 8% chirp relative to the ideal sech^2 pulse shape. This improvement is attributed to the more complex VECSEL chip design, with better GDD balancing, and a standard antiresonant SESAM.

This section has described the successful demonstration of 1:1.3 modelocking of the SESAM-VECSEL combination, depicted as the orange milestone in Fig. 1. The next milestone involves the integration of the pump-DBR and its performance in both cw and modelocking operations, represented by the light green and green milestones in Fig. 1. This will be discussed in the next section.

B. Pump-DBR Integration, Continuous Wave Performance and Modelocking

The next step involves incorporating an additional DBR optimized for the pump wavelength and angle of incidence (Fig. 1, light green milestone). This mirror requires materials with the highest possible refractive index contrast while avoiding any absorption of the pump wavelength. To achieve this, we use the material combination of $AlAs_{0.08}Sb_{0.92}$/ $Al_{0.15}Ga_{0.85}AsSb$.

Fig. 5(a) illustrates the design of a VECSEL chip with a pump-DBR. The bottom mirror remains the same as described in Section III-A—a 19-pair GaSb/ $AlAs_{0.08}Sb_{0.92}$ DBR, highly reflective for the lasing wavelength. On top, there is a 9-pair DBR optimized for reflecting the pump wavelength of 1470 nm at its angle of incidence of 45° in air. The active region is the same as for the GDD-balanced chip, consisting of 5x3 $In_{0.27}Ga_{0.73}Sb$ QWs with $Al_{0.15}Ga_{0.85}AsSb$ spacer layers (Fig. 3(a), (b)). The top AR-coating section has the same number of layers but a slightly different material sequence to achieve a flat GDD for this chip.

This new VECSEL chip remains antiresonant for the laser wavelength, with a node of the electric field intensity at the interface between semiconductor and Si_3N_4. In contrast, a microcavity is formed between this interface and the pump-DBR. Thus, the field intensity of the pump is now increased within the structure, with more pronounced nodes and antinodes. For this simulation, the pump-absorbing properties of the semiconductor

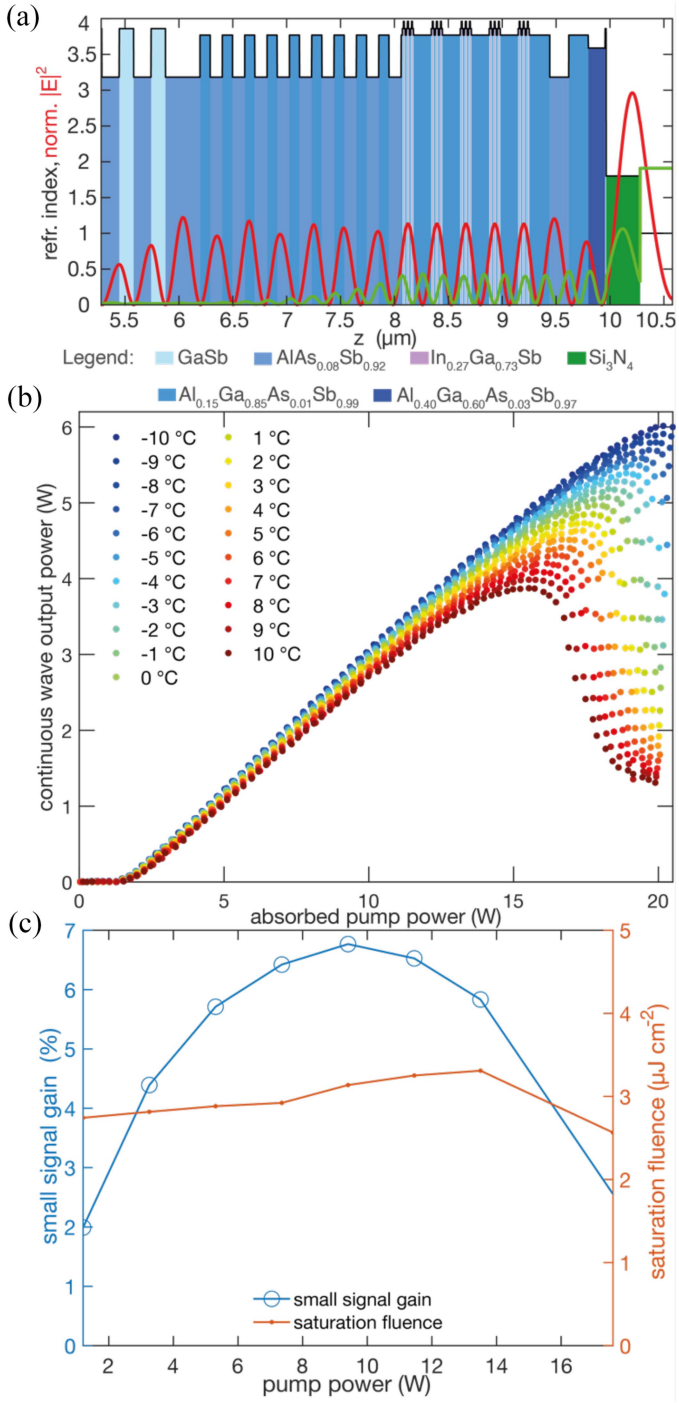

Fig. 5. Design characteristics of a VECSEL chip incorporating a pump-DBR. (a) Design of the active region, showing the refractive index of the materials at the lasing wavelength. The laser DBR is partially depicted. The materials are color-coded with a legend provided at the bottom. The normalized field intensity enhancement is shown for the lasing wavelength (red) and the pump wavelength (green) at their respective angles of incidence. (b) CW power slopes recorded with a 1470-nm pump at a diameter of 394 × 300 μm^2. The pump is elliptically shaped due to the 45° angle of incidence. The heatsink temperature is indicated by color, ranging from blue to red. (c) Pump-dependent parameters extracted from the gain saturation measurement at 2065 nm using 100-fs pulses. The pump is focused to a spot size of 400 μm^2. No elliptical beam shaping is performed in this setup, and the angle of incidence is around 30°. The saturation fluence remains constant at 3 μJ/cm^2, and the small signal gain peaks at a pump power of 10 W, achieving almost 7% small signal gain.

have been disregarded to obtain a clearer view of the pump light propagation within the structure. Investigations of different placements of the pump-DBR, which altered the microcavity resonance of the pump light, led to the conclusion that an arrangement where the pump laser is resonant results in more efficient and higher power cw performance.

Fig. 5(b) shows the power slopes recorded in cw operation for this VECSEL chip using a straight linear cavity and an output coupler with a 1.8% transmission and a 100-mm radius of curvature. The cavity length was 80 mm, and the chip was pumped at a 45° angle of incidence using a 1470-nm DILAS 40-W diode bar with an M^2 value of 96. The pump beam was collimated with cylindrical lenses for elliptical beam shaping, resulting in a projected round pump spot with a diameter of 400 µm on the chip. Power slopes were measured at 21 different temperatures, ranging from −10 °C to 10 °C in 1 °C increments.

The lasing threshold and initial slope efficiency showed no significant variation across the temperature range, indicating that heating effects are negligible in this lower power regime and that the chip can effectively dissipate some heat. However, at higher pump powers and elevated temperatures pronounced rollover effects are observed. These effects appeared more abruptly in chips with a pump-DBR compared to previous measurements [24]. This is likely due to heating-induced shifts in the pump-DBR and its microcavity resonance, which then abruptly reduce device efficiency. This hypothesis is supported by the observation of significant increases in reflected pump power at higher pump levels, suggesting a combination of reduced pump-DBR efficiency and decreased pump absorption.

At −10 °C, the highest measured average output power was 6 W, achieved with an absorbed pump power of 20.2 W, resulting in an optical-to-optical efficiency of 30%. This efficiency surpasses previously reported values for similar structures as shown in Fig. 2, even those with intracavity heatspreaders. Note that this figure shows results at various heatsink temperatures, with some lasers achieving nearly the same efficiency at +20 °C. Additional difficulties for more detailed comparison arise from the fact that power slopes are reported as a function of either absorbed or incident pump power. For incident pump power, the efficiency still remains above 27% for our new VECSEL, making backside-cooled 2–µm VECSELs competitive with the more expensive front-side-cooled VECSELs in this material system. This can be considered an unexpected positive outcome, because it was previously believed that this material system required more intensive cooling than backside cooling alone could provide.

By recording a spectrum at each point in the power slopes as shown in Fig. 5(b), we determined the wavelength change over heatsink temperature at constant pump power and the wavelength change over pump power at constant heatsink temperature. Dividing these values yields a thermal resistance of 1.9 K/W, which is slightly lower than that of a device with a hybrid metal-semiconductor mirror and less than half the thickness of this new VECSEL chip [37].

It is important to note that this new VECSEL chip is not optimized for cw operation. Potential improvements include increasing the pump spot diameter and laser mode to reduce thermal load. Additionally, this device uses an antiresonant design with a field intensity enhancement close to 1, as opposed to a resonant design, which can reach values of 4. However, resonant devices typically have smaller tunability due to their fixed microcavity resonance and are unsuitable for modelocking because of their strongly varying GDD at the lasing resonance.

Fig. 5(c) illustrates the results from linear and nonlinear characterization for this new VECSEL chip using a 120-fs probe laser and a 1470-nm, 15-W pump diode bar. Detailed methodology and data evaluation for this measurement technique are available in a previous study [24]. Measurements were performed at a wavelength of 2065 nm at a heatsink temperature of 5 °C.

The saturation fluence remained constant at 3 µJ/cm^2, only decreasing when the chip was pumped into the rollover regime. Nonsaturable losses were minimal, around 0.1%, and the rollover parameter was measured at 1.2 mJ/cm^2. Notably, the chip exhibits small-signal gain values of nearly 7%, a substantial improvement compared to chips without a pump-DBR.

The excellent cw performance positions this new VECSEL on par with chips featuring intracavity heatspreaders. Additionally, the improved gain saturation and high small-signal gain further establish its suitability for modelocking.

This new VECSEL chip design is modelocked in a V-cavity configuration by an intracavity SESAM, as shown in the inset of Fig. 6(a). indicating cavity length, temperatures, and output coupler details. This experiment corresponds to the second last, green milestone in Fig. 2. The standard two-QW SESAM uses a SiO_2 topcoating to reduce the field intensity enhancement in the structure from 1 to 0.5, allowing a stronger focus on the SESAM without reaching rollover.

Fig. 6(a) shows the optical spectrum centered at 2057 nm with a FWHM of 6.3 nm. The spectrum appears clean, though a slight asymmetry to the right suggests that the GDD is not entirely flat. Additionally, the bandwidth is narrower than previously recorded for 300-fs pulses from the GDD optimized VECSEL, indicating picosecond pulses. Fig. 6(b) presents the microwave spectrum focused on the first harmonic. The repetition rate is 3.03 GHz, with a signal-to-noise ratio exceeding 70 dB, indicating clean mode-locking. Only minimal side peaks are observed. The broad-scan microwave spectrum shows equal power in the higher harmonics, decreasing only above the diode cutoff of 10 GHz. The autocorrelation indicates that the pulses are 1.09 ps long and follow a sech^2 shape with a 1.6 x sech^2 chirp compared to transform limited pulses. The output power is 122 mW at a pump power of 9.7 W, demonstrating that the power is increased with the pump-DBR chips even in modelocking.

For shorter femtosecond pulse generation, further efforts for GDD optimization and growth error reduction would be required. The power can be scaled to over 500 mW with this chip, though fundamental modelocking is lost at higher powers, leading to side pulses or multipulsing, as previously described for 1-µm VECSEL chips [16]. This limitation could be improved by increasing the inverse saturable absorption on the SESAM as multipulsing instabilities occur close to rollover.

The next step is integrating the absorber to achieve a MIXSEL, as indicated by the dark green milestone in Fig. 1. The new VECSEL chip design with GDD optimization and pump-DBR integration discussed in this paper facilitated the first MIXSEL chip by incorporating a saturable absorber layer, consisting of

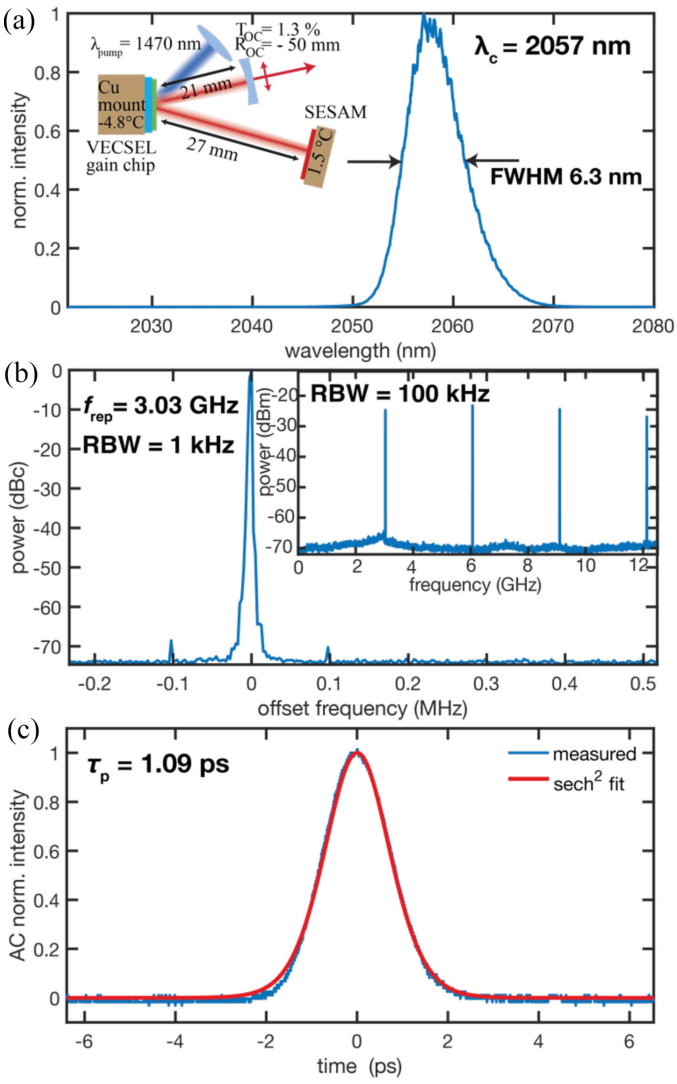

Fig. 6. Modelocking characteristics of a VECSEL chip incorporating both optimized GDD and integrated pump-DBR. (a) Optical spectrum centered around 2057 nm with a full-width half-maximum of 6.3 nm. (b) Microwave spectrum recorded using a 10-GHz photodiode at a resolution bandwidth of 1 kHz, zoomed in on the first harmonic, indicating a repetition rate of 3.03 GHz. The inset displays the full span of the microwave spectrum, showing the higher harmonics. (c) Autocorrelation trace revealing a pulse duration of 1.09 ps, along with a fitted sech^2 function.

a single InGaSb quantum well embedded within GaSb barriers in between the laser and pump DBR. This demonstrates the effective functionality of the pump-DBR. The specifics of this integration, along with its modelocking performance in single and dual-comb operation, have been previously reported and discussed in detail [21].

The following section concludes the paper by presenting a proof-of-principle application for this dual-comb MIXSEL, showcasing a spectroscopy application at 2 μm using this highly integrated chip.

IV. Dual-Comb MIXSEL Spectroscopy

Frequency combs at longer wavelength have been extensively studied on different platforms in single and also dual-comb operation [71], [72], [73]. With the semiconductor platform longer wavelength in the pulsed regime can also be achieved by nonlinear frequency generation [74]. A promising application of long-wavelength semiconductor disk lasers is dual-comb spectroscopy (DCS) of gases [75]. In this technique, the frequency comb is transmitted through a gas medium, imprinting the gas's distinct absorption features onto the optical comb lines. DCS converts this spectroscopic information from the optical domain to the electronic domain by interferometrically combining a pair of combs at a beam splitter and detecting the outputs with a fast photodiode. The heterodyne beating between the combs produces a unique microwave comb line for each pair of optical lines, thus mapping the optical transmission spectrum to the microwave domain. This spectrum can be observed by performing a Fourier transform on the measured time trace.

One challenge in DCS is that the microwave comb line frequencies can fluctuate due to laser noise, necessitating suppression or correction of these fluctuations. A technologically appealing solution is to correct these fluctuations digitally while keeping the optical setup as simple as possible. One effective approach is to generate both combs within the same cavity arrangement. Such dual-comb modelocking solutions, known as single-cavity dual-comb lasers, were first demonstrated several years ago [17], [32], [76], [77], [78], [79]. In [17] an intracavity birefringent crystal enabled the simultaneous modelocked operation of both polarization states of a single MIXSEL cavity. This method of dual-comb generation reduces complexity by sharing components and can also mitigate noise by utilizing a common mechanical path and pump source.

We envisage compact and simple MIXSEL cavities targeting specific wavelength bands in the short-wave infrared and mid-infrared wavelength regions by leveraging semiconductor band gap engineering. These lasers could offer broad terahertz frequency spans, fine spectral sampling at a few gigahertz intervals, microsecond measurement times, and flexible choice of wavelengths. A notable application for such frequency combs is high-speed spectroscopic measurements of dynamic targets, a field of significant interest [80], [81], [82], [83]. For instance, dual-comb systems have been employed to simultaneously measure thousands of absorption lines with update rates as rapid as 4 μs. This capability is crucial for monitoring and understanding the mechanisms of chemical reactions [82], [84], non-repetitive protein reactions [80], [85], and combustion processes [86], [87].

Compared to sources based on nonlinear frequency conversion such as optical parametric oscillators (OPOs), the MIXSEL offers a significantly more compact solution. Therefore, in the rest of this section we present a proof-of-principle demonstration to validate the potential of GaSb-based MIXSELs for dual-comb spectroscopy measurements beyond 2 μm.

In this study, we demonstrate DCS of CO_2 vapor using our dual-comb MIXSEL system, which operates around 2030 nm and overlaps with prominent CO_2 absorption lines. The experimental setup is shown in Fig. 7(a), where the source is the dual-comb MIXSEL located at the bottom left, as reported previously [21]. There are two spatially separated beams emerging from the same cavity. An inverted biprism placed at Brewster's angle

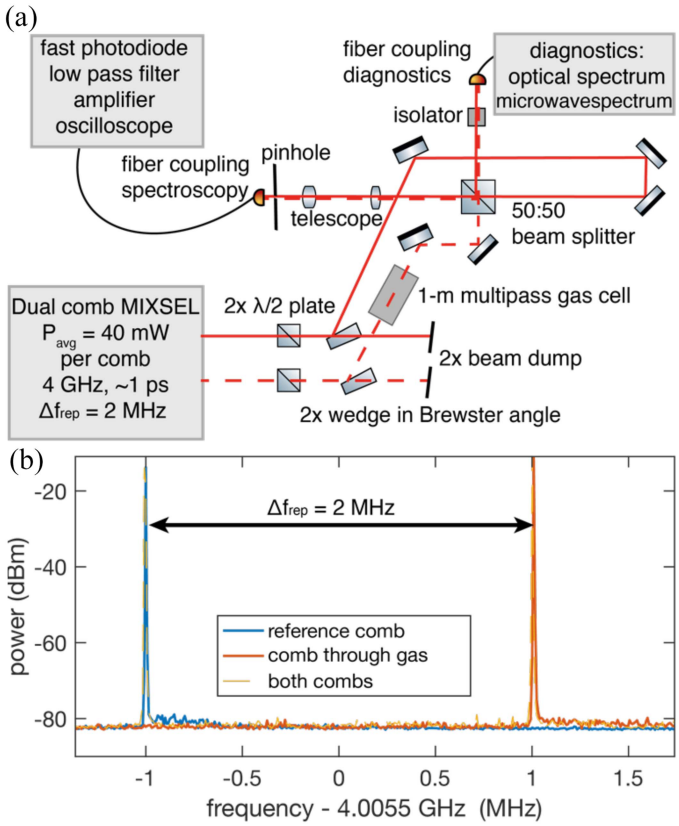

Fig. 7. Proof-of-Principle Spectroscopy Setup. (a) DCS setup, with spatially separated combs represented by solid and dashed lines. (b) Microwave spectrum captured using a fast photodiode, focused on the first harmonic. The individual comb spectra are shown in blue and red, while their combined spectrum is in yellow. An arrow marks the difference in repetition rates between the combs.

spatially multiplexes the cavity. By simultaneously pumping two non-overlapping spots on the semiconductor chip, both resonant cavity paths can be brought to lasing. Each cavity path traverses a different amount of material, resulting in distinct repetition rates. This difference in repetition rates can be tuned by translating the biprism. The beams are individually attenuated using a half-wave plate and a wedged YAG window positioned at Brewster's angle. This setup achieves reflection-based attenuation giving between 0 and 28% of the initial power and strictly s-polarized light. The power is limited to 4.2 mW through the gas cell, preventing saturation effects.

One comb passes through a compact multipass gas cell (Thorlabs MG1C/M-P01), with an optical path length of 1.028 m. The gas cell is filled with CO_2 at a pressure of 1 atm. Both beams are then recombined using a wedged 50:50 beam splitter. One of the recombined beams is mode-matched and coupled into a fiber leading to a fast photodiode (ET-5000F). The resulting photocurrent signal is low-pass filtered (Mini-Circuits SLP-2400+), amplified with a low noise amplifier (RF Bay Inc, ENA-220T), and digitized on an oscilloscope (Teledyne LeCroy WavePro254HD). A pinhole in front of the fiber attenuates the beam to 0.48 mW per comb, preventing nonlinearities in the photodiode.

The other recombined beam is directed to the diagnostic systems, which include an optical spectrum analyzer and a microwave spectrum analyzer. To avoid Fabry-Perot etalon effects, wedged optics are used throughout the setup, with the exception of the half-wave plates. Angle-polished connector (APC) fibers are employed, including at the photodiode, where the fiber was manually repolished to an angled surface to minimize reflections.

The spatial multiplexing technique allows for tuning the difference in repetition rates by adjusting the height of the intracavity biprism. We selected a repetition rate difference of approximately 2 MHz, balancing fast measurement capability and coherent averaging while avoiding aliasing, given the high laser repetition rate. Fig. 7(b) presents the microwave spectrum, overlaying the individual combs with the combined spectrum, zoomed in on the first harmonic. The arrow indicates the difference in repetition rates, and the center frequency of 4 GHz is marked on the x-axis.

The MIXSEL chip was maintained at 10 °C and was pumped with 4.9 W of 1470-nm pump light per comb, resulting in output powers of 44 mW and 38 mW for the two combs, respectively. Fig. 8(a) displays the resulting optical spectra for the individual combs and their combination. Although there is substantial spectral overlap, the spectral shapes are not entirely identical. This discrepancy could be addressed by enhancing wafer processing quality. Notably, the CO_2 absorption lines are visible on the optical spectrum of the red comb even without dual-comb analysis.

The DCS measurements are derived from a 200-ms-long time trace recorded on the oscilloscope. The raw data consists of about 400000 interferogram periods in total. To obtain comb line resolved measurements it is important to track the phase fluctuations of these interferograms. Reducing the noise by a shared cavity arrangement is beneficial for this tracking, as is operation with a large repetition rate difference Δf_{rep} since this implies that the underlying laser noise is sampled frequently (at a rate of Δf_{rep}). Solid-state dual-comb lasers with gigahertz repetition rates have proven well-suited for coherently averaged dual comb spectroscopy [22], [79]. In this work, the shared MIXSEL cavity and the high repetition rate difference of 2 MHz enable coherent averaging even without an enclosure around the laser cavity.

While the full trace is compatible with coherent averaging, to explore the MIXSEL's potential for high-speed spectroscopic measurements we select only the first 16 interferograms of the data, corresponding to a measurement time of just 8 µs. The averaging algorithm uses the carrier envelope phase of each interferogram to compensate for frequency shifts of one microwave comb line, and it uses the interferogram arrival times to compensate for changes in Δf_{rep}. After phase and timing compensation the interferogram signals constitute a Fourier series whose Fourier components correspond to microwave comb lines.

The resulting dual-comb spectrum and absorption lines are shown in Figs. 8(b) and (c), respectively. Several etalon-like features have been removed from the coherently averaged time trace, and a fixed frequency shift has been applied in order to line

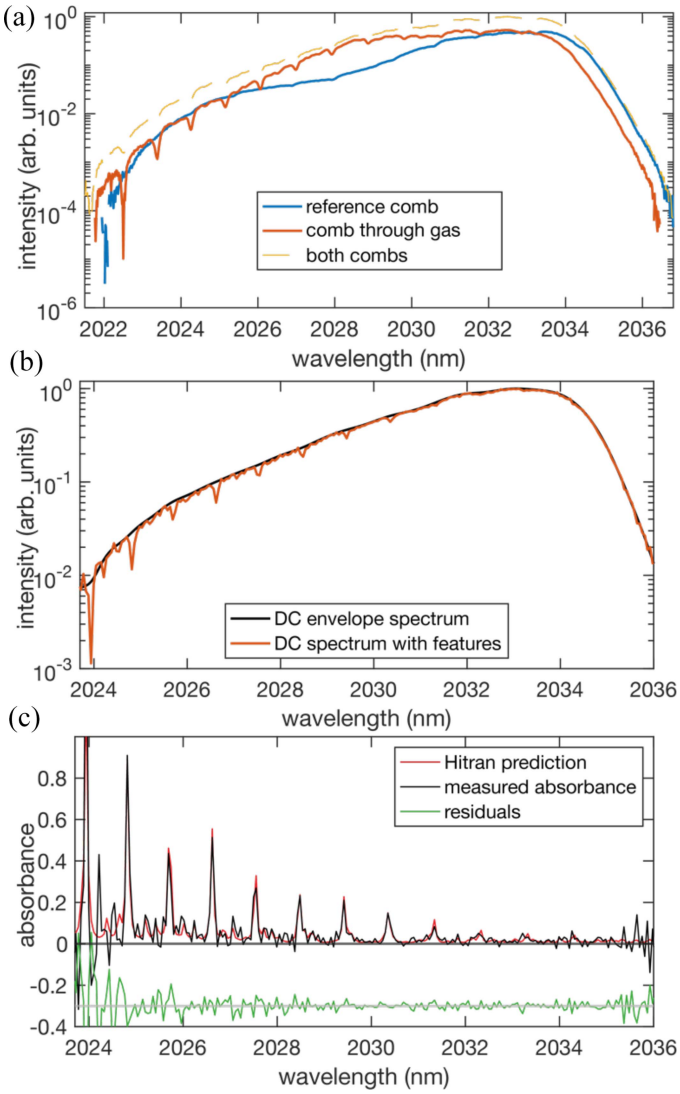

Fig. 8. Proof-of-Principle Spectroscopy Measurement. (a) Optical spectrum of the individual and combined combs, recorded using an optical spectrum analyzer (resolution 0.1 nm), corresponding to the combs in Fig. 7b. (b) Dual-comb spectrum (red line) obtained from Fourier transforming 8 µs of the coherently-averaged time-domain trace. The CO_2 absorption features are clearly visible on the spectrum. The black line is a spectral envelope calculated via a time-gating approach. (c) Inferred absorbance spectrum compared with the HITRAN database prediction. Residuals are shown in green.

up the microwave comb line features with spectroscopic features predicted by the HITRAN database [88]. The observed absorption features are consistent with the database. This measurement represents the first demonstration of DCS using a MIXSEL at a wavelength beyond 2 µm.

V. Conclusion and Outlook

Recent advancements in optically pumped semiconductor disk lasers (VECSELs) operating in the short-wave infrared (SWIR) range, specifically using the GaSb material system, have demonstrated significant progress. These developments span bandgap engineering between 1.97-2.78 µm, power scaling, and single-frequency operation, with an increasing research emphasis on applications in quantum optics and as pump sources for mid-infrared technologies [5], [6], [7], [61].

Our contributions to this field include demonstrating the effectiveness of backside cooling for high-power operation around 2 µm, approaching output powers and efficiencies to those with top-cooled intracavity heatspreaders [24], [37] when operated at only slightly lower heatsink temperatures. This innovation is critical for modelocking since intracavity heatspreaders often present challenges for stable modelocked operation.

In this review, we outline key achievements necessary for the realization of a MIXSEL (Modelocked Integrated eXternal-cavity Surface Emitting Laser) at 2 µm. Initially, we present a design for a group-delay dispersion (GDD) balanced VECSEL chip, achieving transform-limited operation with 331 fs pulses and 30 mW of power in fundamental modelocking. This design enables modelocking with equal mode sizes on both the gain medium (VECSEL) and the absorber (SESAM), facilitating the antiresonant design of an integrated absorber (MIXSEL).

Further advancements include the development and integration of a distributed Bragg reflector optimized for pump light (pump-DBR). This innovation prevents pump light from reaching the absorber quantum well in a MIXSEL, enhancing continuous-wave (cw) performance. VECSEL chips with pump-DBR exhibit up to 6 W of output power and 30% optical-to-optical efficiency at −10 °C, surpassing even devices with intracavity heat spreaders.

These chips have been characterized for gain and investigated in modelocking cavities, demonstrating picosecond operation with 144 mW of output power in fundamental modelocking. Power scaling up to 500 mW is achievable, although fundamental modelocking stability is compromised at higher powers due to multipulse instabilities.

We also conducted proof-of-principle spectroscopy measurements of CO_2, showcasing the dual-comb MIXSEL's potential for accurate spectroscopy with rapid acquisition times as short as 8 µs. These measurements, performed with a table-top MIXSEL exposed to environmental noise, underscore the capability of compact systems for ambient pressure gas sensing in the SWIR range.

Looking ahead, cw operation should target emission wavelengths beyond 3 µm using type-II quantum wells (QWs), which are common in interband cascade lasers and have been explored in optically pumped systems in the near infrared [57]. SESAM development should focus on increasing inverse saturable absorption (F_2) and understanding interband time constants and their precise engineering. These advancements will facilitate broader power scaling of VECSELs and potentially shorter pulses, paving the way for MIXSELs operating in the femtosecond range at wavelengths beyond 2 µm, enabling the spectroscopic analysis of a variety of gases in the molecular fingerprint region.

Acknowledgment

The authors would like to thank FIRST clean room facility at ETH Zürich.

REFERENCES

[1] M. Kuznetsov, F. Hakimi, R. Sprague, and A. Mooradian, "High-power (>0.5-W CW) diode-pumped vertical-external-cavity surface-emitting semiconductor lasers with circular TEM00 beams," *IEEE Photon. Technol. Lett.*, vol. 9, no. 8, pp. 1063–1065, Aug. 1997, doi: 10.1109/68.605500.

[2] B. Heinen et al., "106 W continuous-wave output power from vertical-external-cavity surface-emitting laser," *Electron. Lett.*, vol. 48, no. 9, pp. 516–517, Apr. 2012, [Online]. Available: https://digital-library.theiet.org/content/journals/10.1049/el.2012.0531

[3] T. L. Wang et al., "Quantum design strategy pushes high-power vertical-external-cavity surface-emitting lasers beyond 100 W," *Laser Photon. Rev.*, vol. 6, no. 5, pp. L12–L14, 2012, doi: 10.1002/lpor.201200034.

[4] M. Guina, A. Rantamäki, and A. Härkönen, "Optically pumped VECSELs: Review of technology and progress," *J. Phys. D: Appl. Phys.*, vol. 50, no. 38, Aug. 2017, Art. no. 383001, doi: 10.1088/1361-6463/aa7bfd.

[5] S. C. Burd et al., "VECSEL systems for quantum information processing with trapped beryllium ions," *J. Opt. Soc. Amer. B*, vol. 40, no. 4, pp. 773–781, Apr. 2023, doi: 10.1364/JOSAB.475467.

[6] D. M. Fairbank et al., "Absolute frequency measurements of the D lines in 9Be+ using a single trapped Ion," *Phys. Rev. Lett.*, vol. 131, no. 9, Sep. 2023, Art. no. 093001, doi: 10.1103/PhysRevLett.131.093001.

[7] T. O. Höhn, E. Staub, G. Brochier, N. D. Oppong, and M. Aidelsburger, "State-dependent potentials for the 1S0 and 3P0 clock states of neutral ytterbium atoms," *Phys. Rev. A*, vol. 108, no. 5, Nov. 2023, Art. no. 053325, doi: 10.1103/physreva.108.053325.

[8] S. Hoogland et al., "Passively mode-locked diode-pumped surface-emitting semiconductor laser," *IEEE Photon. Technol. Lett.*, vol. 12, no. 9, pp. 1135–1137, Sep. 2000, doi: 10.1109/68.874213.

[9] B. W. Tilma et al., "Recent advances in ultrafast semiconductor disk lasers," *Light: Sci. Appl.*, vol. 4, no. 7, Jul. 2015, Art. no. 310, doi: 10.1038/lsa.2015.83.

[10] D. Waldburger et al., "High-power 100 fs semiconductor disk lasers," *Optica*, vol. 3, no. 8, pp. 844–852, Aug. 2016, doi: 10.1364/OPTICA.3.000844.

[11] U. Keller and A. C. Tropper, "Passively modelocked surface-emitting semiconductor lasers," *Phys. Rep.*, vol. 429, no. 2, pp. 67–120, Jun. 2006, doi: 10.1016/j.physrep.2006.03.004.

[12] B. Rudin et al., "High-power MIXSEL: An integrated ultrafast semiconductor laser with 6.4 W average power," *Opt. Exp.*, vol. 18, no. 26, pp. 27582–27588, Dec. 2010, doi: 10.1364/oe.18.027582.

[13] D. J. H. C. Maas et al., "Vertical integration of ultrafast semiconductor lasers," *Appl. Phys. B: Lasers Opt.*, vol. 88, no. 4, pp. 493–497, Sep. 2007, doi: 10.1007/s00340-007-2760-1.

[14] M. Mangold et al., "Pulse repetition rate scaling from 5 to 100 GHz with a high-power semiconductor disk laser," *Opt. Exp.*, vol. 22, no. 5, pp. 6099–6107, Mar. 2014, doi: 10.1364/oe.22.006099.

[15] V. J. Wittwer et al., "High-power integrated ultrafast semiconductor disk laser: Multi-Watt 10 GHz pulse generation," *Electron. Lett.*, vol. 48, no. 18, pp. 1144–1145, Aug. 2012, doi: 10.1049/el.2012.2405.

[16] D. Waldburger et al., "Multipulse instabilities of a femtosecond SESAM-modelocked VECSEL," *Opt. Exp.*, vol. 26, no. 17, pp. 21872–21886, Aug. 2018, doi: 10.1364/OE.26.021872.

[17] S. M. Link et al., "Dual-comb modelocked lasers," *Opt. Exp.*, vol. 23, no. 5, pp. 5521–5531, Aug. 2015, doi: 10.1364/oe.23.005521.

[18] S. M. Link, D. J. H. C. Maas, D. Waldburger, and U. Keller, "Dual-comb spectroscopy of water vapor with a free-running semiconductor disk laser," *Science*, vol. 356, no. 6343, pp. 1164–1168, Jun. 2017, doi: 10.1126/science.aam7424.

[19] J. Nürnberg et al., "An unstabilized femtosecond semiconductor laser for dual-comb spectroscopy of acetylene," *Opt. Exp.*, vol. 27, no. 3, pp. 3190–3199, Feb. 2019, doi: 10.1364/oe.27.003190.

[20] J. K. Franks, "What is eye safe?," in *Eyesafe Lasers: Components, Systems, and Applications*. Bellingham, WA, USA: SPIE, Apr. 1991, pp. 2–8, doi: 10.1117/12.43840.

[21] M. Gaulke et al., "Gigahertz semiconductor laser at a center wavelength of 2 µm in single and dual-comb operation," *Opt. Exp.*, vol. 32, no. 1, pp. 26–39, Jan. 2024, doi: 10.1364/OE.503035.

[22] C. R. Phillips et al., "Coherently averaged dual-comb spectroscopy with a low-noise and high-power free-running gigahertz dual-comb laser," *Opt. Exp.*, vol. 31, no. 5, pp. 7103–7119, Feb. 2023, doi: 10.1364/OE.479356.

[23] J. Heidrich et al., "324-fs pulses from a SESAM modelocked backside-cooled 2-µm VECSEL," *IEEE Photon. Technol. Lett.*, vol. 34, no. 6, pp. 337–340, Mar. 2022, doi: 10.1109/LPT.2022.3156181.

[24] M. Gaulke et al., "High average output power from a backside-cooled 2-µm InGaSb VECSEL with full gain characterization," *Opt. Exp.*, vol. 29, no. 24, pp. 40360–40373, Nov. 2021, doi: 10.1364/OE.438157.

[25] C. G. E. Alfieri, D. Waldburger, J. Nürnberg, M. Golling, and U. Keller, "Sub-150-fs pulses from an optically pumped broadband modelocked integrated external-cavity surface emitting laser," *Opt. Lett.*, vol. 44, no. 1, pp. 25–28, Jan. 2019, doi: 10.1364/ol.44.000025.

[26] C. G. E. Alfieri et al., "Mode-Locking instabilities for High-Gain semiconductor disk lasers based on active submonolayer quantum dots," *Phys. Rev. Appl.*, vol. 10, no. 4, Oct. 2018, Art. no. 044015, doi: 10.1103/PhysRevApplied.10.044015.

[27] O. D. Sieber et al., "Experimentally verified pulse formation model for high-power femtosecond VECSELs," *Appl. Phys. B: Lasers Opt.*, vol. 113, no. 1, pp. 133–145, Oct. 2013, doi: 10.1007/s00340-013-5449-7.

[28] A. Karim, S. Bjorlin, J. Piprek, and J. E. Bowers, "Long-wavelength vertical-cavity lasers and amplifiers," *IEEE J. Sel. Topics Quantum Electron.*, vol. 6, no. 6, pp. 1244–1253, Nov./Dec. 2000, doi: 10.1109/2944.902174.

[29] P. Holl et al., "Recent advances in power scaling of GaSb-Based semiconductor disk lasers," *IEEE J. Sel. Topics Quantum Electron.*, vol. 21, no. 6, pp. 324–335, Nov./Dec. 2015, doi: 10.1109/JSTQE.2015.2414919.

[30] P. Holl et al., "GaSb-Based 2.0 µm SDL with 17W output power at 20 °C," *Electron. Lett.*, vol. 52, no. 21, pp. 1794–1795, Oct. 2016, doi: 10.1049/el.2016.2412.

[31] A. Härkönen et al., "Modelocked GaSb disk laser producing 384 fs pulses at 2 µm wavelength," *Electron. Lett.*, vol. 47, no. 7, pp. 454–456, Mar. 2011, doi: 10.1049/el.2011.0253.

[32] J. Pupeikis et al., "Spatially multiplexed single-cavity dual-comb laser," *Optica*, vol. 9, no. 7, pp. 713–716, Jul. 2022, doi: 10.1364/optica.457787.

[33] J. Heidrich et al., "Full optical SESAM characterization methods in the 1.9 to 3-µm wavelength regime," *Opt. Exp.*, vol. 29, no. 5, pp. 6647–6656, Mar. 2021, doi: 10.1364/OE.418336.

[34] B. Ö. Alaydin et al., "Bandgap engineering, monolithic growth, and operation parameters of GaSb-based SESAMs in the 2–2.4 µm range," *Opt. Mater. Exp.*, vol. 12, no. 6, pp. 2382–2394, Jun. 2022, doi: 10.1364/ome.459232.

[35] N. Schulz, J. M. Hopkins, M. Rattunde, D. Burns, and J. Wagner, "High-brightness long-wavelength semiconductor disk lasers," *Laser Photon. Rev.*, vol. 2, no. 3, pp. 160–181, 2008, doi: 10.1002/lpor.200710037.

[36] A. Laurain, L. Cerutti, M. Myara, and A. Garnache, "2.7-µm m Single-frequency TEM00 low-threshold Sb-based diode-pumped external-cavity VCSEL," *IEEE Photon. Technol. Lett.*, vol. 24, no. 4, pp. 246–248, Feb. 2012, doi: 10.1109/LPT.2011.2177252.

[37] N. Huwyler et al., "3-W output power from a 2-µm InGaSb VECSEL using a hybrid metal-semiconductor Bragg reflector," *Opt. Mater. Exp., OME*, vol. 13, no. 3, pp. 833–842, Mar. 2023, doi: 10.1364/OME.485694.

[38] N. Hempler et al., "20 W, quasi-cw GaSb-based semiconductor disk laser," in *Proc. Lasers, Sources Related Photonic Devices, OSA Tech. Dig. Ser. (CD)*, Optical Society of America, Jan. 2010, Paper ATuA14, doi: 10.1364/assp.2010.atua14.

[39] B. Rösener et al., "Continuous-wave room-temperature operation of a 2.8 µm GaSb-based semiconductor disk laser," *Opt. Lett.*, vol. 36, no. 3, pp. 319–321, Feb. 2011, doi: 10.1364/ol.36.000319.

[40] M. Guina et al., "GaSb-based compounds tailored for MID-IR disk lasers," in *Proc. Solid State Lasers XVIII: Technol. Devices*, Bellingham, WA, USA, Feb. 2009, pp. 376–385, doi: 10.1117/12.816221.

[41] B. Rosener et al., "GaSb-Based optically pumped semiconductor disk laser using multiple gain elements," *IEEE Photon. Technol. Lett.*, vol. 21, no. 13, pp. 848–850, Jul. 2009, doi: 10.1109/LPT.2009.2019260.

[42] B. Rösener et al., "GaSb-based optically pumped semiconductor disk lasers emitting in the 2.0-2.8 µm wavelength range," *Proc. SPIE*, vol. 7578, pp. 250–257, Feb. 2010, doi: 10.1117/12.842148.

[43] J. Nikkinen, J. Paajaste, R. Koskinen, S. Suomalainen, and O. G. Okhotnikov, "GaSb-Based semiconductor disk laser with 130-nm tuning range at 2.5 µm," *IEEE Photon. Technol. Lett.*, vol. 23, no. 12, pp. 777–779, Jun. 2011, doi: 10.1109/LPT.2011.2122249.

[44] T. Töpper et al., "High-power 2.0 µm semiconductor disk laser—Influence of lateral lasing," *Appl. Phys. Lett.*, vol. 100, no. 19, May 2012, Art. no. 192107, doi: 10.1063/1.4714512.

[45] J. Paajaste et al., "High-power and broadly tunable GaSb-based optically pumped VECSELs emitting near 2 µm," *J. Cryst. Growth*, vol. 311, no. 7, pp. 1917–1919, Mar. 2009, doi: 10.1016/j.jcrysgro.2008.10.071.

[46] J.-M. Hopkins et al., "High-power, (AlGaIn)(AsSb) semiconductor disk laser at 2 µm," *Opt. Lett.*, vol. 33, no. 2, pp. 201–203, Jan. 2008, doi: 10.1364/ol.33.000201.

[47] S. Kaspar et al., "Linewidth narrowing and power scaling of Single-Frequency 2.X µm GaSb-Based semiconductor disk lasers," *IEEE J. Quantum Electron.*, vol. 49, no. 3, pp. 314–324, Mar. 2013, doi: 10.1109/JQE.2013.2242431.

[48] S. Kaspar et al., "Recent advances in 2-µm GaSb-based semiconductor disk laser—Power scaling, narrow-linewidth and short-pulse operation," *IEEE J. Sel. Topics Quantum Electron.*, vol. 19, no. 4, Jul./Aug. 2013, Art. no. 1501908, doi: 10.1109/JSTQE.2013.2244568.

[49] N. Schulz et al., "Resonant optical in-well pumping of an (AlGaIn)(AsSb)-based vertical-external-cavity surface-emitting laser emitting at 2.35 µm," *Appl. Phys. Lett.*, vol. 91, no. 9, Aug. 2007, Art. no. 091113, doi: 10.1063/1.2773970.

[50] J. P. Perez, A. Laurain, L. Cerutti, I. Sagnes, and A. Garnache, "Technologies for thermal management of mid-IR Sb-based surface emitting lasers," *Semicond. Sci. Technol.*, vol. 25, no. 4, Mar. 2010, Art. no. 045021, doi: 10.1088/0268-1242/25/4/045021.

[51] M. Devautour et al., "Thermal management for high-power single-frequency tunable diode-pumped VECSEL emitting in the near- and mid-IR," *IEEE J. Sel. Topics Quantum Electron.*, vol. 19, no. 4, Jul./Aug. 2013, Art. no. 1701108, doi: 10.1109/JSTQE.2013.2245104.

[52] A. Härkönen et al., "1-W antimonide-based vertical external cavity surface emitting laser operating at 2-µm," *Opt. Exp.*, vol. 14, no. 14, pp. 6479–6484, Jul. 2006, doi: 10.1364/oe.14.006479.

[53] T. Eales et al., "Auger recombination in type I GaInAsSb/GaSb lasers and its variation with wavelength in the 2-3 µm range," presented at Proc. 2017 Eur. Conf. Lasers Electro-Opt. Eur. Quantum Electron. Conf., Munich Germany, Jun. 25—29, Jun. 2017, Paper CB_2_6. Accessed: May 24, 2024, [Online]. Available: https://opg.optica.org/abstract.cfm?uri=CLEO_Europe-2017-CB_2_6

[54] K. S. Gadedjisso-Tossou, S. Belahsene, M. A. Mohou, E. Tournié, and Y. Rouillard, "Recombination channels in 2.4–3.2 µm GaInAsSb quantum-well lasers," *Semicond. Sci. Technol.*, vol. 28, no. 1, Dec. 2012, Art. no. 015015, doi: 10.1088/0268-1242/28/1/015015.

[55] J. R. Meyer, C. A. Hoffman, F. J. Bartoli, and L. R. Ram-Mohan, "Type-II quantum-well lasers for the mid-wavelength infrared," *Appl. Phys. Lett.*, vol. 67, no. 6, pp. 757–759, Aug. 1995, doi: 10.1063/1.115216.

[56] I. Vurgaftman et al., "Interband cascade lasers," *J. Phys. D: Appl. Phys.*, vol. 48, no. 12, Mar. 2015, Art. no. 123001, doi: 10.1088/0022-3727/48/12/123001.

[57] C. Möller et al., "Type-II vertical-external-cavity surface-emitting laser with Watt level output powers at 1.2 µm," *Appl. Phys. Lett.*, vol. 108, no. 7, Feb. 2016, Art. no. 071102, doi: 10.1063/1.4942103.

[58] C. Lammers et al., "Gain spectroscopy of a type-II VECSEL chip," *Appl. Phys. Lett.*, vol. 109, no. 23, Dec. 2016, Art. no. 232107, doi: 10.1063/1.4971333.

[59] M. C. Schuchter, N. Huwyler, M. Golling, M. Gaulke, and U. Keller, "2-µm 1.5-W optically pumped semiconductor membrane laser," *IEEE Photon. Technol. Lett.*, vol. 36, no. 8, pp. 543–546, Apr. 2024, doi: 10.1109/LPT.2024.3377261.

[60] S. Adler et al., "Continuous-tunable single-frequency 2 µm GaSb-based thin device semiconductor disk laser," in *Proc. Conf. Lasers Electro-Opt. Europe Eur. Quantum Electron. Conf. (CLEO/Europe-EQEC)*, Jun. 2017, p. 1, doi: 10.1109/CLEOE-EQEC.2017.8086342.

[61] M. Rattunde, P. Holl, and J. Wagner, "Single-frequency and high power operation of 2–3 micron VECSEL," in *Vertical External Cavity Surface Emitting Lasers*, USA: Wiley, 2021, pp. 63–107, doi: 10.1002/9783527807956.ch3.

[62] A. Garnache, A. Liu, L. Cerutti, and A. Campargue, "Intracavity laser absorption spectroscopy with a vertical external cavity surface emitting laser at 2.3 µm: Application to water and carbon dioxide," *Chem. Phys. Lett.*, vol. 416, no. 1–3, pp. 22–27, 2005, doi: 10.1016/j.cplett.2005.09.028.

[63] N. Hempler et al., "Semiconductor disk laser pumped Cr^{2+}:Znse lasers," *Opt. Exp.*, vol. 17, no. 20, pp. 18136–18141, Sep. 2009, doi: 10.1364/OE.17.018136.

[64] P. Kucirek et al., "A single-frequency Ho:YLF pulsed laser with frequency stability better than 500 kHz," *Proc. SPIE*, vol. 10082, Mar. 2017, pp. 305–310, doi: 10.1117/12.2253722.

[65] K. Scholle et al., "SDL In-band Pumped Q-switched 2.1 µm Ho:YAG Laser," presented at Proc. Conf. Lasers Electro-Opt., San Jose, CA, USA Jun. 5–10, 2016, Paper STu4M.2, doi: 10.1364/CLEO_SI.2016.STu4M.2.

[66] P. Holl et al., "GaSb-based VECSEL for high-power applications and Ho-pumping," in *Proc. SPIE*, Bellingham, WA, vol. 10087, pp. 31–37, Feb. 2017, doi: 10.1117/12.2254287.

[67] A. Hildenbrand et al., "Laser damage of the nonlinear crystals Cd-SiP2 and ZnGeP2 studied with nanosecond pulses at 1064 and 2090 nm," *Proc. SPIE*, vol. 53, no. 12, Aug. 2014, Art. no. 122511, doi: 10.1117/1.OE.53.12.122511.

[68] A.-R. Bellancourt et al., "Low saturation fluence antiresonant quantum dot SESAMs for MIXSEL integration," *Opt. Exp.*, vol. 17, no. 12, pp. 9704–9711, Jun. 2009, doi: 10.1364/OE.17.009704.

[69] D. Lorenser et al., "50-GHz passively mode-locked surface-emitting semiconductor laser with 100-mW average output power," *IEEE J. Quantum Electron.*, vol. 42, no. 8, pp. 838–847, Aug. 2006, doi: 10.1109/JQE.2006.878183.

[70] D. J. H. C. Maas et al., "Growth parameter optimization for fast quantum dot SESAMs," *Opt. Exp.*, vol. 16, no. 23, pp. 18646–18656, Nov. 2008, doi: 10.1364/OE.16.018646.

[71] T. Fortier and E. Baumann, "20 years of developments in optical frequency comb technology and applications," *Commun. Phys.*, vol. 2, no. 1, Dec. 2019, Art. no. 153, doi: 10.1038/s42005-019-0249-y.

[72] C. Zhang et al., "Recent advances and outlook in single-cavity dual comb lasers," *Photonics*, vol. 10, no. 2, 2023, Art. no. 221, doi: 10.3390/photonics10020221.

[73] A. Schliesser, N. Picqué, and T. W. Hänsch, "Mid-infrared frequency combs," *Nature Photon.*, vol. 6, no. 7, pp. 440–449, 2012, doi: 10.1038/nphoton.2012.142.

[74] R. Rockmore, A. Laurain, J. V. Moloney, and R. J. Jones, "Offset-free mid-infrared frequency comb based on a mode-locked semiconductor laser," *Opt. Lett.*, vol. 44, no. 7, pp. 1797–1800, Apr. 2019, doi: 10.1364/OL.44.001797.

[75] I. Coddington, N. Newbury, and W. Swann, "Dual-comb spectroscopy," *Optica*, vol. 3, no. 4, pp. 414–426, Apr. 2016, doi: 10.1364/optica.3.000414.

[76] X. Zhao et al., "Picometer-resolution dual-comb spectroscopy with a free-running fiber laser," *Opt. Exp.*, vol. 24, no. 19, pp. 21833–21845, Sep. 2016, doi: 10.1364/OE.24.021833.

[77] R. Liao et al., "Dual-comb spectroscopy with a single free-running thulium-doped fiber laser," *Opt. Exp.*, vol. 26, no. 8, pp. 11046–11054, Apr. 2018, doi: 10.1364/OE.26.011046.

[78] S. Mehravar, R. A. Norwood, N. Peyghambarian, and K. Kieu, "Real-time dual-comb spectroscopy with a free-running bidirectionally mode-locked fiber laser," *Appl. Phys. Lett.*, vol. 108, no. 23, Jun. 2016, Art. no. 231104, doi: 10.1063/1.4953400.

[79] N. B. Hébert et al., "Self-corrected chip-based dual-comb spectrometer," *Opt. Exp.*, vol. 25, no. 7, pp. 8168–8179, Apr. 2017, doi: 10.1364/OE.25.008168.

[80] M. J. Norahan et al., "Microsecond-Resolved infrared spectroscopy on nonrepetitive protein reactions by applying caged compounds and quantum cascade laser frequency combs," *Anal. Chem.*, vol. 93, no. 17, pp. 6779–6783, May 2021, doi: 10.1021/acs.analchem.1c00666.

[81] D. A. Long et al., "Nanosecond time-resolved dual-comb absorption spectroscopy," *Nature Photon.*, vol. 18, no. 2, pp. 127–131, Feb. 2024, doi: 10.1038/s41566-023-01316-8.

[82] N. H. Pinkowski et al., "Dual-comb spectroscopy for high-temperature reaction kinetics," *Meas. Sci. Technol.*, vol. 31, no. 5, Mar. 2020, Art. no. 055501, doi: 10.1088/1361-6501/ab6ecc.

[83] G. Zhang, R. Horvath, D. Liu, M. Geiser, and A. Farooq, "QCL-based dual-comb spectrometer for Multi-Species measurements at high temperatures and high pressures," *Sensors*, vol. 20, no. 12, Jan. 2020, Art. no. 3602, doi: 10.3390/s20123602.

[84] N. Hoghooghi et al., "GHz repetition rate mid-infrared frequency comb spectroscopy of fast chemical reactions," *Optica*, vol. 11, no. 6, pp. 876–882, Jun. 2024, doi: 10.1364/OPTICA.521655.

[85] J. L. Klocke et al., "Single-Shot Sub-microsecond Mid-infrared spectroscopy on protein reactions with quantum cascade laser frequency combs," *Anal. Chem.*, vol. 90, no. 17, pp. 10494–10500, Sep. 2018, doi: 10.1021/acs.analchem.8b02531.

[86] A. D. Draper et al., "Broadband dual-frequency comb spectroscopy in a rapid compression machine," *Opt. Exp.*, vol. 27, no. 8, pp. 10814–10825, Apr. 2019, doi: 10.1364/OE.27.010814.

[87] A. S. Makowiecki et al., "Mid-infrared dual frequency comb spectroscopy for combustion analysis from 2.8 to 5 µm," *Proc. Combustion Inst.*, vol. 38, no. 1, pp. 1627–1635, Jan. 2021, doi: 10.1016/j.proci.2020.06.195.

[88] I. E. Gordon et al., "The HITRAN2020 molecular spectroscopic database," *J. Quantitative Spectrosc. Radiative Transfer*, vol. 277, Jan. 2022, Art. no. 107949, doi: 10.1016/j.jqsrt.2021.107949.

Marco Gaulke was born in Mannheim, Germany, in 1993. He received the bachelor's and master's degrees from the Karlsruhe Institute of Technology, Karlsruhe, Germany, in 2015 and 2018, respectively, and the Ph.D. degree from the Ultrafast Laser Physics Group, ETH Zürich, Zürich, Switzerland, in 2023. He is currently a physicist working in laser physics and semiconductor technology. He was the recipient of the German Academic Scholarship Foundation's scholarship from the Karlsruhe Institute of Technology. During his academic journey, his bachelor's thesis focused on modeling physisorption processes. For his master's thesis, he examined electroluminescence of carbon nanotubes at low temperatures. He continues his research at ETH Zurich as a Postdoctoral Researcher, concentrating on advancing semiconductor-based VECSEL and MIXSEL technologies further into the infrared spectrum.

Maximilian Constantin Schuchter was born in Florida, USA, in 2000. He received the Bachelor of Science degree in interdisciplinary sciences from ETH Zürich, Zürich, Switzerland, focusing on physics and chemistry, and the Master of Science degree from in interdisciplinary sciences from ETH Zurich, with a GPA of 5.63/6. He is currently working toward the Ph.D. degree in laser physics and semiconductor technology. Since August 2022, he has also been working toward the joint doctoral degree with ETH Zurich, Switzerland and Tampere University, Tampere, Finland. In his bachelor's thesis he worked on the "Characterisation of Membrane Modes". He conducted his master's thesis at the University of California, Berkeley, CA, USA, and was titled "Attosecond Noncollinear Four-Wave-Mixing Spectroscopy." His research focuses on developing Semiconductor Saturable Absorber Mirrors (SESAMs) and high-power, ultrashort mid-IR semiconductor lasers. Supervised by Prof. Ursula Keller at ETH Zurich and Prof. Mircea Guina at Tampere University. He has already presented his findings at international conferences and was the recipient of the Best Student Presentation Award for his research on the "Investigation on Wavelength, Strain, and Barrier Materials in SWIR InGaSb SESAMs."

Nicolas Huwyler was born in Altdorf, Switzerland, in 1996. He received the M.Sc. degree in physics in 2021 from ETH Zürich, Zürich, Switzerland, where he is currently working toward the Ph.D. degree with the Ultrafast Laser Physics Group, focusing on GaSb-based VECSEL and MIXSEL technologies operating between 2 and 3 μm.

Matthias Golling was born in Sulz/Neckar, Germany, in 1971. He received the Dipl.-Ing. and Dr.-Ing. degrees in electrical engineering from the University of Ulm, Ulm, Germany, in 1997 and 2004, respectively. In 1996, he was with NTT Optoelectronic Labs., Ibaraki, Japan, where he investigated erbium-doped waveguides. Since 2002, he has been with the Institute of Quantum Electronics, ETH Zurich, Switzerland. During the first years at ETH, his research interests focused on the crystal growth of high-speed electronic and optoelectronic devices with molecular beam epitaxy. In the following years, he concentrated on the growth of laser structures and saturable absorber structures (SESAMs) on GaAs.s. Since 2019, his research has broadened to the growth of GaSb-based materials. He is now developing VECSEL and MIXSEL for the 2.xx micrometer wavelength range.

Benjamin Willenberg was born in Goch, Germany, in 1988. He received the B.Sc. degree in mathematics and the M.Sc. degree in physics from Göttingen University, Göttingen, Germany, in 2013 and 2014, respectively, and the Ph.D. degree in physics from ETH Zürich, Zürich, Switzerland, for work in the fields of strong-field ionization and attosecond science, as well as highly efficient high-power frequency conversion from the NIR to the DUV. Since 2019, he has been a Postdoctoral Researcher with the Ultrafast Laser Physics group of Prof. Keller at ETH Zurich, focusing on the development of low-noise single-cavity dual-comb oscillators and their applications in science and industry.

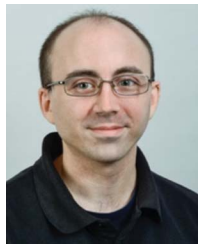

Christopher R. Phillips received M.S. and Ph.D. degrees in electrical engineering from Stanford University, Stanford, CA, USA, in 2009 and 2012, respectively. At Stanford, he worked on nonlinear optical devices for pulsed and continuous-wave photonic applications. Following his PhD, he moved to ETH Zürich, Zürich, Switzerland, to work in the Ultrafast Laser Physics group, supported by a Marie Curie fellowship, on optical parametric chirped pulse amplification. After the fellowship, he continued at ETH, where he broadened his research interests, and is now the Senior Project Leader for the solid-state frequency combs subgroup. He has coauthored about 60 journal publications and 120 conference papers. His current research interests include modelocked lasers and parametric oscillators with low-noise, high repetition rate, and high power; applications of dual optical frequency combs; and numerical modeling of nonlinear-optical systems. He is a senior member of the Optica.

Ursula Keller (Fellow, IEEE) received the Physics "Diplom" from ETH Zürich, Zürich, Switzerland, in 1984, and the Ph.D. degree from Stanford University, Stanford, CA, USA, in 1989. She was a Member of Technical Staff (MTS) at AT&T Bell Laboratories from 1989 to 1993, a Visiting Miller Professor at the University of California, Berkeley, Berkeley, CA, USA, in 2006, and a Visiting Professor at the Lund Institute of Technologies, Lund, Sweden, in 2001. She has been a tenured Professor of Physics with ETH Zürich, since 1993, and was the Director of the Swiss Multi-Institute NCCR MUST program in Ultrafast Science from 2010 to 2022. She has been a co-founder and board member for Time-Bandwidth Products (acquired by JDSU in 2014) and for a venture-capital-funded telecom company GigaTera (acquired by Time-Bandwidth in 2003). She was a member of the research council of the Swiss National Science Foundation from 2014-2018. She is the founding president of the ETH Women Professors Forum. She has authored or coauthored more than 520 journal publications and according to Google Scholar, an h-index of 120 with more than 55 000 citations. In 2022, she authored a new graduate textbook on "Ultrafast Lasers" published by Springer Verlag. She has supervised and graduated 96 Ph.D. students. Her research group focuses on exploring and pushing the frontiers of ultrafast science and technology. She was the recipient of awards include the Swiss Science Prize Marcel Benoist (2022) – the "Swiss Nobel Prize," OSA Frederic Ives Medal/Jarus W. Quinn Prize (2020) – OSA's (resp. OPTICA's) highest award for overall distinction in optics, SPIE Gold Medal (2020) – SPIE's highest honor, IEEE Edison Medal (2019), IEEE Photonics Award (2018), European Inventor Award for lifetime achievement (2018), two ERC advanced grants (2012 and 2018), member of the U.S. National Academy of Sciences, Royal Swedish Academy of Sciences, German Academy Leopoldina, and Swiss Academy of Technical Sciences.